

Microfluidic study of the chemotactic response of *Escherichia coli* to amino acids, signaling molecules and secondary metabolites

Krisztina Nagy, Orsolya Sipos, Sándor Valkai, Éva Gombai, Orsolya Hodula, Ádám Kerényi, Pál Ormos, and Péter Galajda

Citation: *Biomicrofluidics* **9**, 044105 (2015); doi: 10.1063/1.4926981

View online: <http://dx.doi.org/10.1063/1.4926981>

View Table of Contents: <http://scitation.aip.org/content/aip/journal/bmf/9/4?ver=pdfcov>

Published by the [AIP Publishing](#)

Articles you may be interested in

[Inducing chemotactic and haptotactic cues in microfluidic devices for three-dimensional in vitro assays](#)
Biomicrofluidics **8**, 064122 (2014); 10.1063/1.4903948

[Simplified prototyping of perfusable polystyrene microfluidics](#)
Biomicrofluidics **8**, 046501 (2014); 10.1063/1.4892035

[Modeling and validation of autoinducer-mediated bacterial gene expression in microfluidic environments](#)
Biomicrofluidics **8**, 034116 (2014); 10.1063/1.4884519

[Using surface plasmon resonance imaging to study bacterial biofilms](#)
Biomicrofluidics **8**, 021804 (2014); 10.1063/1.4867739

[Covalently immobilized biomolecule gradient on hydrogel surface using a gradient generating microfluidic device for a quantitative mesenchymal stem cell study](#)
Biomicrofluidics **6**, 024111 (2012); 10.1063/1.4704522

Did your publisher get
18 MILLION DOWNLOADS in 2014?
AIP Publishing did.



THERE'S POWER IN NUMBERS. Reach the world with AIP Publishing.



Microfluidic study of the chemotactic response of *Escherichia coli* to amino acids, signaling molecules and secondary metabolites

Krisztina Nagy,^{a)} Orsolya Sipos,^{a)} Sándor Valkai, Éva Gombai, Orsolya Hodula, Ádám Kerényi, Pál Ormos, and Péter Galajda^{b)}
Institute of Biophysics, Biological Research Centre of the Hungarian Academy of Sciences, Temesvári krt. 62, H-6726 Szeged, Hungary

(Received 23 March 2015; accepted 2 July 2015; published online 15 July 2015)

Quorum sensing and chemotaxis both affect bacterial behavior on the population level. Chemotaxis shapes the spatial distribution of cells, while quorum sensing realizes a cell-density dependent gene regulation. An interesting question is if these mechanisms interact on some level: Does quorum sensing, a density dependent process, affect cell density itself via chemotaxis? Since quorum sensing often spans across species, such a feedback mechanism may also exist between multiple species. We constructed a microfluidic platform to study these questions. A flow-free, stable linear chemical gradient is formed in our device within a few minutes that makes it suitable for sensitive testing of chemoeffectors: we showed that the amino acid lysine is a weak chemoattractant for *Escherichia coli*, while arginine is neutral. We studied the effect of quorum sensing signal molecules of *Pseudomonas aeruginosa* on *E. coli* chemotaxis. Our results show that N-(3-oxododecanoyl)-homoserine lactone (oxo-C12-HSL) and N-(butryl)-homoserine lactone (C4-HSL) are attractants. Furthermore, we tested the chemoeffector potential of pyocyanin and pyoverdine, secondary metabolites under a quorum sensing control. Pyocyanin is proved to be a weak attractant while pyoverdine are repellent. We demonstrated the usability of the device in co-culturing experiments, where we showed that various factors released by *P. aeruginosa* affect the dynamic spatial rearrangement of a neighboring *E. coli* population, while surface adhesion of the cells is also modulated. © 2015 AIP Publishing LLC. [<http://dx.doi.org/10.1063/1.4926981>]

INTRODUCTION

Bacteria can effectively cope with their chemically heterogeneous environment and find the optimal living conditions (e.g., nutrient sources) and places by responding to chemical signals. Through chemotaxis, bacteria are able to detect the concentration gradients of chemoeffector molecules and actively alter their motility patterns accordingly.^{1,2} In heterogeneous environments, motility and chemotaxis can provide essential advantages for bacteria.¹

Research in the last two decades revealed the importance and also the mechanisms of cell–cell signaling in bacteria.³ In quorum sensing, for example, cells secrete and detect signaling molecules.⁴ Above a threshold signal concentration, gene expression patterns may change resulting in a cell-density dependent response.^{5,6} Multiple quorum sensing circuits and corresponding signaling molecules have been identified in different bacteria. Previous studies in the literature suggest that there is some connection between quorum sensing and motility/chemotaxis.^{7–10} However, these studies mainly deal with the chemoeffector potential of autoinducer 2 (AI-2) that is predominantly involved in interspecies communication. No studies have been published about the chemoeffector potential of N-acyl homoserine lactones (AHLs), which is a

^{a)}K. Nagy and O. Sipos contributed equally to this work.

^{b)}Electronic mail: galajda.peter@brc.mta.hu

large class of quorum signaling molecules involved in communication of Gram-negative bacteria. The relation between quorum sensing and chemotaxis seems particularly important if we consider that both phenomena play a crucial role in bacterial infections.^{11–16}

Pseudomonas aeruginosa (*P. aeruginosa*) has two main quorum sensing systems.^{17–21} The LasI/R and RhII/R quorum sensing circuits are hierarchically organized and regulated via N-(3-oxododecanoyl)-homoserine lactone (oxo-C12-HSL) and N-(butyryl)-homoserine lactone (C4-HSL), respectively. Both of these molecules belong to the class of AHLs. While these signaling molecules are natural clues for bacteria, it is an interesting question if they could be chemoeffectors (even for other species) at the same time. Since most bacterial species with a quorum sensing system produce a characteristic set of AHLs, these chemicals are mainly treated in the literature as intraspecies signal molecules. Nevertheless, it has been proved that other species are able to sense and respond to them as well. For example, SdiA was identified in *Escherichia coli* (*E. coli*) as a receptor-like protein for the AHL signal interception from other bacteria.^{22–24} Beside AHLs, *P. aeruginosa* secretes several secondary metabolites and assumed signaling molecules such as pyocyanin and pyoverdine that could also act as chemoeffector in mixed co-culture systems.

Pyocyanin is a redox-active secondary metabolite and a virulence factor produced by *P. aeruginosa* with a broad spectrum of antimicrobial activity.²⁵ Pyocyanin biosynthesis, as the production of many other molecules that are used in bacterial communication, is regulated by the quorum sensing system of *P. aeruginosa*.²⁶ Pyocyanin is also known to be a terminal active compound in the quorum sensing network of *P. aeruginosa*.²⁷

Pyoverdine forms a family of extracellular siderophore molecules, produced by *P. aeruginosa* that is important in iron scavenging. Gram-negative bacteria use outer membrane receptors for the uptake of siderophores loaded with ferric ions. It has been shown that *E. coli* FecA and *P. aeruginosa* FpvA belong to the same subfamily of siderophore outer membrane receptors.²⁸ These receptors are able to bind iron-free siderophores, as well as metal loaded ones. It was hypothesized that the role of iron-free siderophore/outer membrane receptor complexes could be relevant in bacterial communication, through which bacteria can gather and share information about their local environment.²⁹ It has also been revealed that bacteria are able to utilize xenosiderophores produced by other bacterial species.³⁰ This supports the idea that siderophores may act as interspecies communication signals.

Earlier capillary assays and chemotaxis plates were used for exploring the foundations of chemotactic behavior of bacteria; however, these techniques have some inherent limitations.³¹ In microfluidic channels and chambers, liquids can be precisely manipulated on the microscopic level and temporally stable gradients can be accurately established. In the last decade, several microfluidic devices were developed for bacterial chemotaxis studies. The majority of these gradient generators rely on fluid flow.^{7,32,33} Although gradients can be established in these devices, in most of the cases, bacteria are only exposed to the gradient for a short time (~20–30 s) as they are carried along with the flowing media. Therefore, weak chemotactic responses may not be detected in these devices. Also, single cell chemotactic measurements are not possible in these flow-based gradient generators. The flow may also cause shear stress on cells, which can influence their behavior. The location dependent flow velocity (e.g., a usually parabolic flow profile) in the channel may result in a hydrodynamic orientation of rod shaped bacteria. This physical process may hinder the chemotactic response.

The above mentioned limitations can be overcome by flow-free gradient generator devices. Two main types of these gradient generators have been developed. Some of them use flow for a short period of time in the test channel,^{34–36} or separately in another microchannel^{37–39,41,42,45} to allow the chemical gradient establishment. Others rely solely on diffusion during gradient formation.^{40,43,44} One of the biggest advantages of the flow-free devices compared to flow based ones is that undisturbed chemotaxis response can be studied in a steady liquid medium for an extended period of time.

However, the flow-free operation also have some limitations. Compared to the timescale needed for the chemotactic response, devices—reported in the literature—require relatively a long period of time to create a stable gradient. Some of the devices require filling or flushing

the side channels or reservoirs for several hours to enable the solvents to diffuse into the porous elements (gel structures).^{42–44,46,47} The timescales span from 30 min to several hours. When the gradient formation is slow, the timescale of chemotactic pattern formation is limited by the time needed for a stable concentration profile to form. For detailed studies of the dynamics of chemotaxis, a fast gradient formation is required. In several flow-free devices, relatively large volumes are filled with gel type materials that separate solvent reservoirs from bacterial test channels.^{41–43,46,47} Solvents diffuse in gels isotropically; therefore, these structures have a substantial buffering capacity. This makes it difficult to carry out experiments where the chemical environment is needed to be altered in time. Furthermore, only part of the gradient, which is formed between the solvent reservoirs, falls within the cellular test channel, and the substantial part of the gradient develops inside the gel structures.

We built a new microfluidic platform where we are able to establish stable, flow-free chemical concentration gradients and address some of the limitations of other flow-free devices. Similarly to some other flow-free gradient generators,^{39–45} stable linear gradients develop in our device based solely on diffusion, without fluid flow in the test channel. We used a solid membrane with directional pores sandwiched between two microfluidic layers. Experiments and model calculations were done to characterize the dynamics of the formation and the stability of the concentration profiles. Due to the high porosity and relatively low thickness of the membrane, the gradient forms and stabilizes fast, within 3 min in our device. The design and assembly realizes some advantages that make this platform appealing for a wide range of experiments. We demonstrated the usability of the device with a well-known chemotactic attractor (aspartate), and a repellent (nickel). Furthermore, we characterized the weak chemotactic response of *E. coli* to lysine that was previously thought to be chemotactically neutral. We studied the chemoeffector potential of important signal molecules in bacterial communication, such as AHLs, pyoverdine, and pyocyanin. The fast gradient formation also makes the device ideal for co-culturing experiments, where the dynamic interaction of physically separated but chemically coupled cell cultures is studied. We demonstrated this by showing chemotactic response in neighboring cultures induced by secreted factors.

MATERIALS AND METHODS

Microfluidic chip design

The schematic representation of the microchip used for flow-free chemical gradient generation in our experiments is shown in Fig. 1. The device consists of two polydimethylsiloxane (PDMS) layers and a porous membrane that is inserted in between.⁵⁴ The upper layer has two large trapezoid shaped reservoirs (the sides of the reservoir are 1.0, 0.5, 0.5, 0.65 cm long, and they each have a volume of $\sim 45 \mu\text{l}$) that were usually loaded by sample medium on one side and a reference medium on the other side. The bottom layer contains a $40 \mu\text{m}$ deep, 1.2 mm wide, and 1 cm long observation channel ($\sim 0.4 \mu\text{l}$ volume). There is an overlapping area between the reservoirs and the observation channel (Fig. 1(b)). This overlapping area runs along the central channel and is designed to be $100 \mu\text{m}$ on both sides. The concentration gradient across the width of the observation channel is generated by diffusion of molecules from one reservoir to the other through the membrane and the central channel. Figure 1(b) shows a representative image of the gradient of a fluorescent dye molecule, pyranine in the observation channel.

Fabrication of the microfluidic device

The gradient generator device was fabricated from PDMS (Dow Corning Corp., Sylgard 184) and aluminum-oxide membrane ($60 \mu\text{m}$ thickness, $0.1 \mu\text{m}$ pore diameter, Anodisc 47, Whatman). Negative master molds were created by using standard photolithography techniques.⁴⁸ For creating the master molds of the channels a SU8–2015 (MicroChem Corporation) layer with $40 \mu\text{m}$ height was spincoated (model P6700, Speciality Coating Systems Inc.) on a silicon wafer. For the masters of the reservoirs, 1 mm thick photoresist layer was created on a

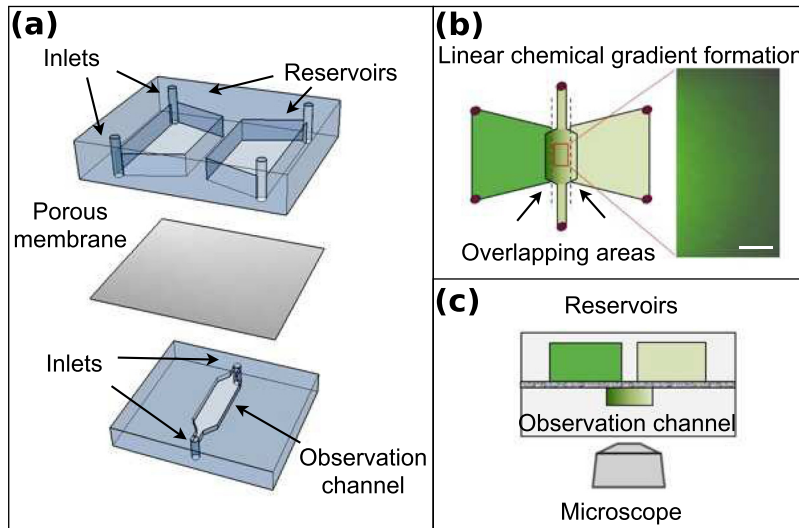


FIG. 1. Schematic representation of the gradient generator microfluidic device (not to scale). (a) A perspective view showing the three sandwiched component of the device. A top layer includes the reservoirs; a bottom layer contains the observation channel. These layers are separated by a porous aluminium-oxide membrane. (b) Top view of the device. Diffusion of molecules between the reservoirs through the membrane and the central channel leads to the formation of a chemical concentration gradient across the channel. The inset shows a fluorescence microscopy image of the central channel with a pyranine concentration gradient. The scale bar is $200\ \mu\text{m}$. (c) Cross sectional view of the device showing the observation of the channel from below (as in an inverted microscope).

coverslip. To achieve better adhesion, the glass surfaces were pretreated by Omnicoat (MicroChem Corporation). Since such a thick photoresist layer can hardly be created by spin-coating, the coverslips were covered directly by SU8–2050. The coverslips were kept on a precisely leveled 95°C hotplate for 3 days in a chemical hood (softbake). The photoresist layers were exposed to UV light (flood exposure source with mask aligner, 500 W Hg lamp, i-line, model 97435, Newport Corporation and Digital Exposure Controller model 68945, Newport Corporation) through transparency film masks (JD Photo-Tools Ltd.). In order to prevent the PDMS from attaching to the SU8 molds, the molds were silanized using tridecafluoro-1,1,2,2-tetrahydrooctyl)trichlorosilane (Gelest Inc.) under vacuum for at least 4 h. Positive replicas were fabricated by molding the PDMS on the master. The cured PDMS (baked at 40°C overnight in an oven) was peeled off and holes for inlets and outlets were punched. A thin layer of PDMS ($6\text{--}10\ \mu\text{m}$) was used to bond the layers and the porous membrane to each other, similar to the method of Chueh *et al.*⁴⁹ The microchips were used without further treatment or surface coating. After filling the observation channel with medium, the assembled device was mounted on a microscope glass slide using fast curing transparent PDMS (WPI Inc.). Then, the reservoirs were also loaded and the inlets/outlets were closed by fast curing PDMS.

Fluorescent dye diffusion experiments

Gradients generated in the device were characterized by using pyranine (Sigma-Aldrich Corp.), a water soluble fluorescent dye. Pyranine was solved in potassium-phosphate buffer ($\text{pH} = 7.0$) at concentrations of $0.1\ \mu\text{M}$ and $1\ \mu\text{M}$. These solutions were used to load one reservoir, while the other one was filled with pure buffer. At the beginning of these experiments, the observation channel was filled with a 1:1 mixture of the buffer and the dye solution, then the left reservoir was filled with buffer and the right reservoir with the dye solution. In long term experiments, the complete filling procedure was done before starting fluorescence time-lapse imaging. In short term experiments, the central channel was filled, then the sample was mounted on the microscope. In order to capture the beginning of the gradient formation, we started the time-lapse imaging before the right and left reservoirs were filled. During the dye diffusion experiments, fluorescence microscopy images of the central channel were taken in

15 s intervals in the first 10 min, 1 min intervals in the next 50 min, 5 min intervals in the next 3 h of the experiments, and hourly afterwards. Control experiments, where pyranine was loaded in the same concentration into both reservoir chambers, were used to calibrate the measured fluorescence intensity in the observation channel with known dye concentrations.

Model calculations

The diffusion of pyranine within the microfluidic device was simulated with the “Transport of Diluted Species” model of Comsol Multiphysics 4.3a software. According to the geometric parameters of the microfluidic device (reservoirs, membrane and observation channel), a two-dimensional model representing the cross section of the device was built and tested. Although the diffusion constant of pyranine in solution is $0.425 \times 10^{-9} \text{ m}^2/\text{s}$, the diffusion through a membrane of 30% porosity was considered by using an effective diffusion constant of $0.1275 \times 10^{-9} \text{ m}^2/\text{s}$. Two kinds of simulations were performed with the computational model: short term (4 h) calculations with higher resolution for examining the formation of the chemical gradient and long term simulations (120 h) for monitoring the stability of the gradient.

Bacterial chemotaxis experiments

For the chemotaxis experiments, we used the *E. coli* HCB33 strain (equal to RP437), which is considered to be wild type for chemotaxis.⁵⁰ This strain was transformed with the pMPMA2-GFPmut2 plasmid⁵¹ for green fluorescent protein (GFP) expression. Control experiments were carried out using *E. coli* HCB437 non-chemotactic, smooth swimming strain,⁵⁰ also carrying the above mentioned plasmid.

Bacteria were grown overnight in 3 ml lysogeny broth (LB) medium supplemented with antibiotics (50 $\mu\text{g}/\text{ml}$ streptomycin and/or 50 $\mu\text{g}/\text{ml}$ ampicillin) at 30 °C in plastic tubes in an incubator shaker (200 rpm). Overnight cultures were diluted back in the morning, and cells at a concentration of OD₆₀₀ (optical density measured at 600 nm) between 0.5 and 0.8 were centrifuged (3000 rpm, 10 min, two times), and resuspended in chemotaxis buffer (CB) (PBS, pH = 7.0, 0.1 mM EDTA, 0.01 mM L-methionine, 10 mM DL-Lactate, 10 mg/ml bovine serum albumin (BSA)) (based on Englert *et al.*⁷). The chemoeffector was added to the bacterial suspension at the mid-point concentration of the gradient. Then, the cells were pipetted into the central channel of the assembled device. As a reference medium, pure CB medium was used in all experiments. All the chemicals used for cell culturing were purchased from Sigma-Aldrich. Furthermore, all the chemoeffectors tested (amino acids, NiSO₄, AHLs, pyocyanin and pyoverdine) were also purchased from Sigma-Aldrich.

As a control, fluorescence images of the bacteria in the channel were taken before loading the reservoirs. The time of loading and closing of the large reservoirs was set to $t=0$ (imaging was started about 2 min later).

Co-culturing experiments

P. aeruginosa PUPa3 cells⁵² were used beside the above mentioned *E. coli* strains in the co-culturing experiments. Overnight cultures grown in LB medium at 30 °C in a shaker incubator, shaken at 200 rpm were diluted 1000 times in 3 ml LB medium supplemented with antibiotics in sterile polystyrene tubes. The cells were grown at 30 °C in a shaker incubator until they reached an optical density of 0.5–0.8 at 600 nm. First, the observation channel was filled with the *E. coli* culture (OD₆₀₀ ~ 0.3). Then, one of the reservoirs was filled with CB medium, and the other one with LB medium containing *P. aeruginosa* bacteria as well (OD₆₀₀ ~ 0.6). The initial cell density of bacteria in the channel was half of the cell density in the reservoir. The appropriate concentration was achieved by diluting the *E. coli* culture in 1:1 ratio with CB medium before loading the channel. During these experiments, all the media contained 10 mg/ml BSA.

Microscopy and image analysis

Fluorescence microscopy was used to visualize the gradient formation in fluorescent dye experiments and record the spatial distribution of bacteria during chemotaxis experiments. All experiments were carried out at 30 °C using a Nikon Eclipse Ti-E inverted microscope (Nikon Inc.) equipped with a home built incubator. A 10 × Nikon Plan Fluor objective, a GFP fluorescence filter set (49002 filter set, Chroma Inc.), a Prior Proscan II motorized stage (Prior Scientific Ltd.) and a LUMEN 200 Pro metal arc lamp (Prior Scientific Ltd.) were part of the microscope setup. Time-lapse imaging was done by an Andor NEO sCMOS camera (Andor Technology plc.), and NIS Elements Ar software (Nikon Inc.) was used for image acquisition and microscope control.

Matlab 2013a (MathWorks Inc.) and ImageJ,⁵³ an open source software package, were used for data processing and image analysis. Background correction was performed on each image using the “rolling ball” algorithm of ImageJ. Manufacturing artifacts of the membranes were visible as small bright spots on the fluorescence images. These spots were masked out and excluded from the image analysis.

We used the asymmetry index A ⁵⁴ to quantify the spatial distribution of bacteria across the width of the observation channel in chemotaxis experiments. For this purpose, the observation channel was divided into two equal areas, and the average fluorescence intensity (which is assumed to be proportional to the cell number) was measured in the left and the right half of the channel (I_{left} and I_{right} , respectively). Then, A is calculated as

$$A = \frac{(I_{left} - I_{right})}{(I_{left} + I_{right})}. \quad (1)$$

The asymmetry index A is zero if the cells distribute equally between both halves of the channel. A is -1 or 1 if all the cells are on the left or right side, respectively. Different spatial distributions yield a value between -1 and 1 . In all the experiments, the left reservoir contained the sample media (sample chamber) and the right one contained pure buffer (reference chamber).

RESULTS AND DISCUSSION

Generation and characterization of gradients

In our microfluidic device, a chemical gradient is generated across the width of the observation channel as a result of diffusion of molecules present in different concentrations in the reservoirs. The generated gradient was tested by filling one reservoir with pyranine solution (left in the microscopy images) and the other reservoir with phosphate buffer at pH = 7.0 (right in the microscopy images). The central channel was filled with a 1:1 mixture of buffer and dye

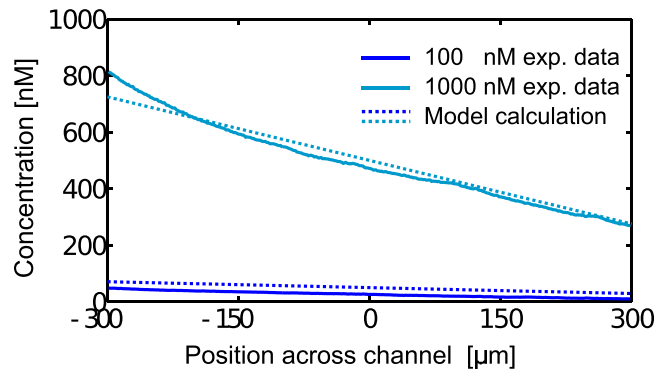


FIG. 2. Concentration profiles of pyranine solutions across the central channel. Solid lines: 1000 nM and 100 nM pyranine solutions loaded in the left reservoir. Dashed lines: results of model calculations.

solutions. We selected a field in the middle of the observation channel (excluding the overlapping areas (Fig. 1(c))), and measured the average intensity profile of this area across the channel. The fluorescence intensity was considered as direct representation of pyranine concentration, and corresponding calibration measurements were performed.

First, we studied the formation and the long term maintenance of the concentration gradient in the device. Figure 2 shows the concentration profile of pyranine across the width of the central channel 1 h after filling the device. The profile is very close to linear (a linear fit provides r^2 values of 0.9907 and 0.9766 in the case of using 100 nM and 1000 nM pyranine solutions). For various experimental applications, it may be desired to precisely control the chemical gradient inside the channel. By loading solutions of different concentrations into the reservoirs, the gradient in the channel can be controlled. We used 100 and 1000 nM pyranine solutions to demonstrate this. Figure 2 shows that a ten times higher dye concentration in the reservoir results in a ten times higher gradient in the channel. The results of a finite element analysis, including the full 3D geometry of the microfluidic device and the diffusion properties of pyranine in water, agree well with the experimental data (Fig. 2). The slope values of the concentration profiles obtained by linear regression are -61 ± 0.6 pM/ μm and -818.5 ± 11.7 pM/ μm when using 100 nM or 1000 nM pyranine solutions, respectively. The model calculations provide slope values of -69.72 ± 0.005 pM/ μm and -749.1 ± 0.005 pM/ μm , which agree well with the experimental results.

We studied the formation and stability of gradients on various timescales. In short term experiments, we filled the central channel with 50 nM pyranine solution and sealed the inlet and outlet holes of the channel. After starting the timelapse recording, we filled the right and left reservoirs with buffer and 100 nM pyranine solution, respectively, and sealed the inlet/outlet holes of the reservoirs. Fig. 3(a) shows the dye concentration across the width of the central channel at various times. After filling the reservoirs, a linear concentration profile formed that changed little after 3 min. This is in a good agreement with the results of model calculations shown in Fig. 3(b). The slope of the concentration profile obtained by linear regression is plotted in time in Fig. 3(c). The graph demonstrates that the gradient formed quickly and stabilized

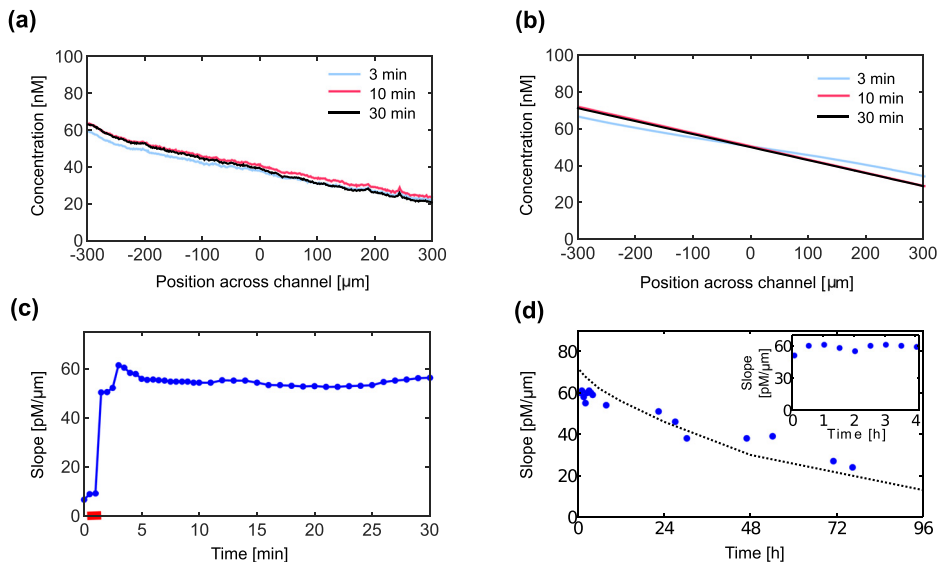


FIG. 3. (a) Concentration profiles of the pyranine solution across the central channel at different times. The times indicated were measured after filling both reservoirs. (b) Model calculations of the concentration profiles of the pyranine solution across the channel at different times. (c) Short term change of the concentration gradient after filling the device. The thick red line on the x axis indicates the time needed to fill both reservoirs. (d) Change of the concentration gradient in the device in time on long timescales. Solid circles: slope of the linear concentration profile in the experiments. Dashed line: result of model calculation.

in about 3 min after the reservoirs were filled. Subsequent fluctuations in the gradient were within 10%.

The quick gradient formation is due to the design of the device and the components used. The membrane has high porosity with directional pores and limited thickness of 60 μm , which both facilitate the diffusion processes forming the gradient. Other devices reported in the literature require relatively long times (from 30 min to several hours) to create a stable gradient. This is often due to the relatively large porous structures that the molecules have to diffuse through. Our experiments also demonstrate that the device is suitable for the fast temporal manipulation of the gradient. By quickly changing the content of the reservoirs, the gradient in the central channel may be altered in minutes. In some other devices, such fast temporal gradient control is not possible due to the buffering capacity of bulky gel structures.^{42–44,46,47}

In typical flow based devices, bacteria are exposed to the gradients for less than a minute.⁷ One advantage of flow-free devices may be that this timescale can be extended for more precise chemotaxis measurements. Therefore, we measured the long term (72 h) change of the gradient in our device. Figure 3(d) shows the change of the pyranine concentration gradient in time in the central channel. We found that after filling a 100 nM pyranine solution into the left reservoir, a 60 pM/ μm gradient was formed within a few minutes and this gradient became stable. On longer timescales, the concentration gradient decreased as the concentration of the dye equilibrated between the two reservoirs. However, this equilibration process is quite slow, due to the relatively large volume of the reservoirs compared to the central channel and also the limited overlapping area between the reservoirs and the channel. The drop in the gradient is about 15% within 24 h. This makes the device suitable for experiments on much longer timescales compared to flow-based microfluidic devices. The membrane used in our device has directional transmembrane pores which assures that diffusion only takes place vertically across, but not laterally within the membrane. This constrained diffusion may ensure a precise, controllable gradient formation. However, in other flow free gradient generator devices made of or incorporating gels, the solutes in the device may diffuse isotropically within the gel based structural elements, creating complex spatial concentration distributions.

Chemotaxis experiments

We demonstrated the usability of our device for chemotaxis studies with chemical gradients of L-aspartate (Asp), a chemoattractant and nickel (Ni^{2+} ions from NiSO_4), a chemorepellent for *E. coli*. Apart from these two well-known chemoeffectors, we tested the chemoeffector potential of L-Arginine monohydrochloride (Arg) and L-Lysine monohydrochloride (Lys) as well. Earlier studies found no chemotactic response of *E. coli* to these two amino acids by using capillary assays and chemotaxis plate methods.^{55,56}

Fluorescence microscopy was used to image GFP expressing bacteria exposed to chemoeffector gradients in the central channel and follow their motile response. As previously, the chemoeffectors of interest in these experiments were loaded into the left reservoir. As a result, the concentration of chemoeffectors decreased from left to right in the central channel where fluorescent bacteria were also placed. By taking thin sections of images of the central channel at subsequent times and plotting one below the other, kymographs of the experiments can be generated. These kymographs demonstrate qualitatively the differences in the dynamics of the chemotactic response to various chemoeffectors. Kymographs of the first 15 min of typical experiments for aspartate and nickel, two strong chemoeffectors, are shown in Figs. 4(a) and 4(b). At the beginning of the experiments, bacteria spread homogeneously across the channel, but within minutes, they started to move towards the left or right side of the channel. After about 8–10 min, almost all bacteria moved to the high Asp (left in Fig. 4(a)) or low Ni^{2+} (right in Fig. 4(b)) concentration side of the channels. The asymmetry index (A) given by Eq. (1) was used to quantitatively characterize the chemotactic response of bacteria to a given chemical gradient. The index correlates with the spatial distribution of cells in the channel and helps not only to analyze the dynamics of the cellular response but also to compare accurately the effect of various chemoeffectors.

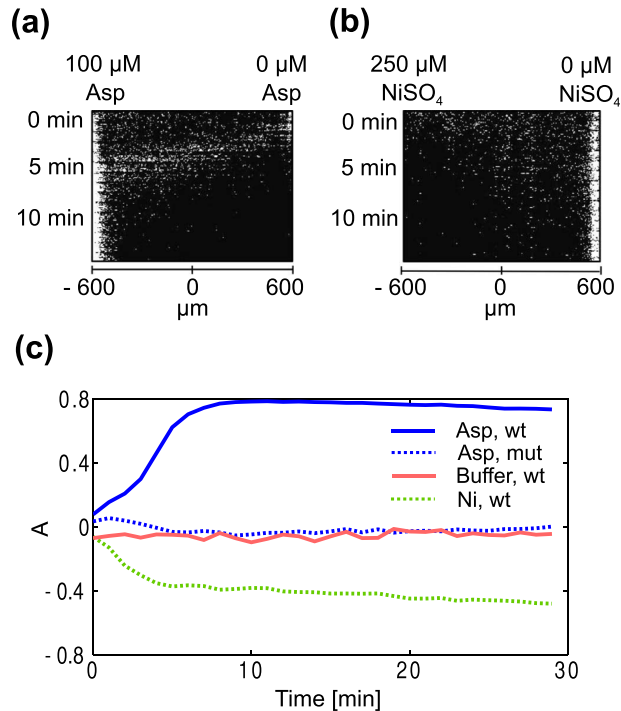


FIG. 4. (a) Kymograph showing the temporal change of the spatial distribution of chemotactic bacteria across the channel in an L-aspartate (a strong attractant) gradient. (b) Kymograph showing the temporal change of the spatial distribution of chemotactic bacteria across the channel in case of a NiSO₄ gradient. Ni²⁺ is a strong repellent. (c) Asymmetry index (A) for bacteria in various chemical gradients. Solid blue line (dark gray in print): chemotactic (wt) bacteria in aspartate gradient, dashed blue line (dark gray in print): non-chemotactic (mutant) bacteria in aspartate gradient, solid red line (light gray in print): chemotactic bacteria in the absence of chemoeffector gradient (in buffer), and dashed green line (light gray in print): chemotactic (wt) bacteria in nickel gradient.

The value of A may vary between -1 and 1 , with the extreme cases of all cells being on the right or left side of the channel. Since in all of our experiments the concentration of the tested chemoeffector decrease from left to right in the channel, we get positive or negative A values for positive or negative chemotactic responses, respectively. Figure 4(c) shows the asymmetry index (A) over time in the case of well-known chemoeffectors. When $100\ \mu\text{M}$ L-aspartate (a strong attractant) is loaded into the left reservoir, A increases quickly and maintains a positive value indicating the positive chemotactic response and the accumulation of cells on the left side. For a gradient of a strong repellent ($250\ \mu\text{M}$ NiSO₄ solution in the left reservoir) A drops below zero quickly after the start of the experiment and stabilizes around -0.5 .

We performed various control experiments, some results are also shown in Figure 4(c). Chemotactic cells in the absence of a chemoeffector gradient (i.e., buffer in both reservoirs, or identical chemoeffector solutions everywhere) did not accumulate on either side of the test channel throughout the time course of the experiment (yielding a near zero A value). Similarly, as expected, non-chemotactic, mutant bacteria also stayed evenly distributed across the channel even in the presence of an L-aspartate or in a NiSO₄ gradient. In the above experiments, the timescale of the chemotactic response to both aspartate and nickel is slower than that of the gradient formation. This indicates that in this device, we are indeed able to measure the dynamics of the chemotactic response itself that is not limited by a slow gradient formation. Altogether, the above mentioned results demonstrate the usability of our microfluidic platform for chemotaxis studies.

Due to the flow-free nature of this microfluidic platform and the stable linear gradients formed within the central channel, we propose that the device is suitable for demonstrating even weak chemotactic responses of the bacteria. The amino acid L-lysine was previously considered neutral for *E. coli* based on capillary chemotaxis assays.⁵⁵ In these earlier experiments,

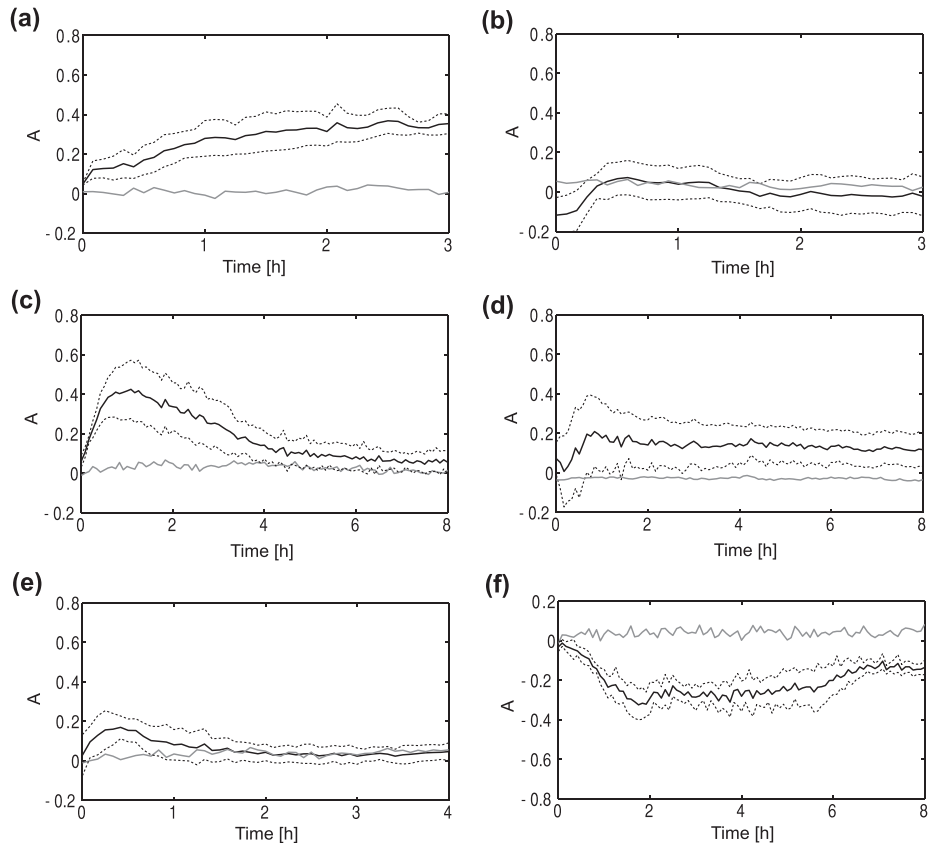


FIG. 5. Asymmetry index for *E. coli* bacteria in amino acid, AHL and secondary metabolite gradients. Continuous black line: average response of chemotactic cells. Dashed lines: standard error. Continuous grey line: response of non-chemotactic cells. (a) Bacteria in lysine gradient. (b) Bacteria in arginine gradient. (c) Bacteria in C4-HSL gradient. (d) Bacteria in oxo-C12-HSL gradient. (e) Bacteria in pyocyanin gradient. (f) Bacteria in pyoverdine gradient.

no chemotactic response was detected, even in gradients created by using lysine concentrations of 100 mM that is higher than physiological. We performed chemotaxis tests with our device using conditions similar to the capillary assay experiments⁵⁵ to see if the sensitivity of our method enables to revealed even a weak response to L-lysine. A 100 mM solution of L-lysine was loaded in the left reservoir. We have observed a slow accumulation of cells on the left side of the channel, although on a much slower timescale than in the case of L-aspartate (three repeated experiments). The asymmetry index shows that in about 1.5 h there were 30% more cells on the left, on the high lysine concentration side (Fig. 5(a)). Thus, both the degree of cellular accumulation and the characteristic timescale suggest a weak chemotactic response to L-lysine by *E. coli*. Control experiments performed using non-chemotactic mutant cells showed no cellular accumulation on either side of the channels (Fig. 5(a)).

L-arginine at the same concentration is similarly presumed to have no chemoeffector potential.⁵⁵ In our experiment (three repeats), we used a 100 mM solution of L-arginine in the left reservoir to create a gradient. The analysis of the bacterial distribution showed that there is no cellular accumulation taking place, and the asymmetry index stayed near zero in the 3 h time-course of the experiment (Fig. 5(b)). A similar behavior was observed in control experiments using non-chemotactic mutants (Fig. 5(b)). Therefore, our results support the previously shown neutrality of L-arginine in *E. coli* chemotaxis.

Chemotaxis and communication signals

Quorum sensing and chemotaxis both affect the behavior of bacteria on the population level. Chemotaxis shapes the spatial distribution patterns of cells, while quorum sensing realizes

a cell-density dependent gene regulation mechanism. Therefore, it is an interesting question if these mechanisms interact on some level, i.e., if the density dependent quorum sensing mechanism affects cell density itself via chemotaxis. Since quorum sensing often spans across species, such a feedback mechanism may also exist in relation of multiple species. We have studied the effect of signal molecules of *P. aeruginosa* on *E. coli* chemotaxis. Since *E. coli* biofilm formation is affected via the quorum sensing regulator SdiA receptor in the presence of certain AHL molecules,²⁴ it is upmost interesting to study the chemoeffector potential of these molecules. Furthermore, we also tested the chemoeffector potential of compounds excreted by *P. aeruginosa* under a quorum sensing control.

The two main quorum sensing systems of *P. aeruginosa*, the Las and Rhl systems, employ 3-oxo-C12-HSL and C4-HSL as signal molecules. *E. coli* cells were investigated in our microfluidic device in the presence of gradients of C4-HSL or 3-oxo-C12-HSL. The maximum concentration of the AHLs in each experiment was 100 μM with a previously shown linear gradient profile, and the experiments were repeated 3–5 times both for the C4-HSL and the oxo-C12-HSL tests. Similar AHL concentrations were measured to exist in *P. aeruginosa* biofilms.⁵⁷ A clear positive chemotactic response was found both in the C4-HSL and the oxo-C12-HSL gradients as demonstrated by the positive values of asymmetry index A (Figs. 5(c) and 5(d)). The cells started to accumulate at the high C4-HSL concentration side of the channel immediately after the exposure to AHL (Fig. 5(c)). The maximum asymmetry in cell distribution ($A = 0.4$) was observed after 1 h. After that, a slow rearrangement of the cell distribution started that resulted in an even spreading of cells after about 6 h. This shows that *E. coli* exhibits a strong but only transient chemotactic response to C4-HSL, and some sort of “adaptation” or “conditioning” leads to the disappearance of this response after several hours. In experiments using non-chemotactic mutant bacteria, no accumulation of cells on either side was seen (Fig. 5(c)). A very similar, but weaker effect was seen for *E. coli* cells in oxo-C12-HSL gradients (Fig. 5(d)). The initial definite positive chemotactic response was followed by the slow leveling off of the spatial distribution of cells. Again, non-chemotactic mutant cells did not respond to the gradient (Fig. 5(d)). The above results suggest that similar mechanisms are behind the chemotactic response to these two distinct AHL molecules; however, further studies are needed to explore the molecular background (e.g., the receptors involved).

The secretion of pyocyanin, a well-known secondary metabolite of *P. aeruginosa*, is regulated by the quorum sensing system. In three repeated experiments, chemotactic *E. coli* cells were exposed to a linear chemical gradient of pyocyanin, where the highest pyocyanin concentration was 50 μM . The used pyocyanin concentration was chosen in agreement with concentrations of purified extracts from cell cultures reported earlier.²⁵ In this case, a weak positive chemotactic response was observed with a peak in the asymmetry index after 30 min (Fig. 5(e)). At that point ($A = 0.2$), approximately 60% of the cells accumulated at the side of the channel with the higher pyocyanin concentration. After half an hour, the cells started to slowly spread out evenly in the whole channel. When non-chemotactic mutant cells were used, bacteria stayed equally distributed over the channel, no accumulation occurred during the experiment (Fig. 5(e)). Based on these observations, we can say, that pyocyanin, a secondary metabolite and virulence factor of *P. aeruginosa*, is a weak chemoattractant for *E. coli*. It has a much lower chemotactic potential than aspartate or the AHLs we tested, but it is still comparable with lysine. It is likely that although pyocyanin may bind to one or more MCP sensory proteins, this interaction is much weaker than in the case of well-known chemoeffectors.

Pyoverdine are extracellular siderophore molecules involved in iron scavenging and are secreted by *P. aeruginosa*. It has been shown before that both *E. coli* and *P. aeruginosa* have receptors for siderophores.⁵⁸ It has been previously proposed that pyoverdine can also act as signaling molecules in a mechanism called pyoverdine signaling⁵⁹ that is also related to virulence. Moreover, pyoverdine biosynthesis is affected by the Las quorum sensing system.⁶⁰ Therefore, we wanted to test experimentally if pyoverdine have any chemotactic potential. In three repeated experiments, we observed wild type chemotactic *E. coli* cells in our microchannel, exposed to a linear gradient of pyoverdine, with a maximum concentration of 20 $\mu\text{g}/\text{ml}$. Similar pyoverdine concentrations were reported previously in cell culture supernatants.⁶¹

A weak negative chemotactic response of *E. coli* was observed, and this response was prolonged compared to that for pyocyanin. Approximately 65% of the cells swam to the lower concentration side of the channel in the first hour of the experiment, and this distribution of cells was maintained for approximately 4–5 h (Fig. 5(f)). Then, cells spread out across the whole channel, but a visible portion of the cells stayed near to the low concentration side even after 8 h. Therefore, we can claim that pyoverdine are weak chemorepellent for *E. coli*. Although the chemotactic response seems to weaken after a few hours, the accumulation of cells is more prolonged compared to pyocyanin. When non-chemotactic mutant cells were used, bacteria stayed equally distributed over the channel, no accumulation occurred during the experiment (Fig. 5(f)).

Interaction of bacterial populations

Due to the usability of our device in long-term experiments, we were able to study the interaction of different bacterial populations in coupled environments. Our setup provides an opportunity for co-culturing different bacterial strains in the reservoirs and the central channel of the microfluidic chip. In this scenario, the populations in the different chambers are physically separated from each other but chemically coupled through the porous membrane of the device. In this configuration, gradients of signal molecules and other secreted biochemical factors form in the central channel during the experiments, and we can observe how cells behave in such heterogeneous environments. The fast action of the device ensures that chemical factors released by one culture in one of the compartments have an almost immediate effect on the neighboring culture. This may be especially important in the case of those chemoeffectors which are only produced transiently in a population.⁸

Previously, we used our microchip to study the interaction of two *E. coli* populations. We found that secreted metabolic compounds from a growing *E. coli* population can cause a strong negative chemotactic response in an adjacent *E. coli* population.⁵⁴ We co-cultured *E. coli* and *P. aeruginosa* cells in our device in order to study the interactions of these physically separated but chemically coupled cultures. *P. aeruginosa* cells in LB medium were loaded into the left reservoir, while the right reservoir was filled with CB medium. The central channel was loaded with *E. coli* cells in 1:1 mixture of the two different medium. The structure of the chip does not allow the direct observation of the *P. aeruginosa* population in the reservoir, only the *E. coli* cells in the central channel were imaged.

During the experiment, the *E. coli* population showed a dynamic spatial rearrangement in the channel. In the first phase of the experiment, *E. coli* cells accumulated on the left side of the channel, adjacent to the *P. aeruginosa* population (Fig. 6(a)). Since the *P. aeruginosa* cells were loaded into the reservoir in LB medium, a nutrient gradient formed in the central channel. It is likely that *E. coli* cells moved along this attractive gradient to the left side. After 2 h, the cells were aggregated at the left side of the channel. We observed that the majority of the *E. coli* cells right next to the *P. aeruginosa* populations adhered to the surface of the microdevice. However, after about 4 h, a small planktonic subpopulation of *E. coli* cells migrated to the right side of the channel, away from the adhered, sessile subpopulation (Figs. 6(a) and 6(b)).

A simple quantitative analysis using the asymmetry index in this case is difficult. Due to the presence of a sessile and a planktonic subpopulation, the spatial distribution of the cells is more complex and the asymmetry index does not capture this.

In order to confirm if chemotaxis plays a role in the dynamic spatial rearrangement of the *E. coli* population, we repeated the experiment with non-chemotactic *E. coli* mutants (Fig. 6(c)). These cells did not accumulate on the side next to *P. aeruginosa* population in the first phase of the experiment; however, a gradual increase in the adhesion of the cells was observed. There was no subsequent migration of a motile subpopulation to the right side in this experiment either. This shows that the initial accumulation of the *E. coli* cells adjacent to the *P. aeruginosa* population, and also the subsequent transmigration away from the *Pseudomonas* population requires the chemotactic capability. In this experiment, a slight variation of cell density was observed across the width of the channel. This is due to a differential growth effect

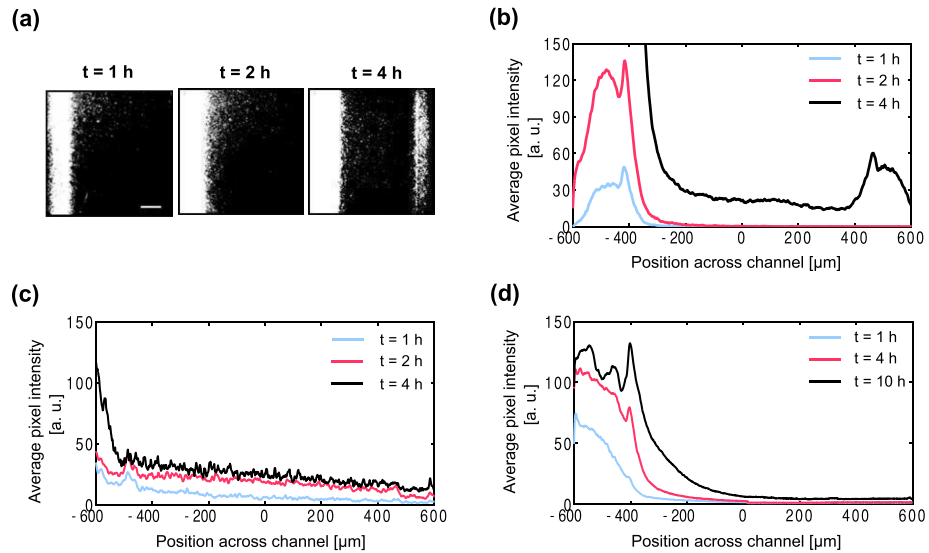


FIG. 6. Co-culturing experiments showing the interaction of adjacent populations. (a) Fluorescence microscopy images of the *E. coli* culture in the channel in the *P. aeruginosa*-*E. coli* co-culturing experiment at different times. Significant surface adhesion of bacteria is observed on the left side of the channel. The scale bar is $200 \mu\text{m}$. (b) Average pixel intensity across the width of the channel representing the distribution of *E. coli* bacteria at different times for the *P. aeruginosa*-*E. coli* co-culturing experiment. (c) Average pixel intensity across the width of the channel representing the distribution of non-chemotactic *E. coli* bacteria at different times for the *P. aeruginosa*-*E. coli* co-culturing control experiment. (d) Average pixel intensity across the width of the channel representing the distribution of *E. coli* bacteria at different times for the control experiment where cell-free pure LB medium was loaded into the left reservoir.

(the spatial variation of the growth rate) that is the consequence of the existence of a nutrient gradient in the channel. Such a differential growth can be observed for the chemotactic cells too (Fig. 6(b)), although there it is mostly covered by the chemotactic pattern formation.

We have also carried out control experiments where only blank LB medium was put into the left reservoir to verify the potential role of the *P. aeruginosa* population in the observed left-to-right migration. In these experiments, the initial accumulation of the cells on the left took place due to the nutrient concentration gradient, but the subsequent transmigration to the right side did not occur. This result suggests that the presence of the *P. aeruginosa* population in the left reservoir was necessary for the left-to-right migration. Although we do not exclude the possibility that factors secreted by *E. coli* may shape the spatial distribution of cells, this does not seem to be the dominating effect in this case.

In order to find out if there is any chemoeffector potential of BSA, or any small compounds originating from BSA degradation, we performed control experiments without using BSA in the media. We have found the same spatial rearrangement of the *E. coli* population in the observational channel as in the original experiments, where BSA was added to the media. Our findings show that the presence of BSA in the media did not affect the chemotactic response of *E. coli*.

Considering the given timescale, we assume that these planktonic *E. coli* cells exhibited negative chemotaxis in response to compounds secreted by the *P. aeruginosa* bacteria. *E. coli* can detect and respond to numerous metabolic products and communication signals produced by *P. aeruginosa*, such as pyocyanin, pyoverdine, AHLs, diketopiperazines,⁶² Pseudomonas quinolone signal.⁶³ As these active compounds play a crucial role in functional multispecies microbial communities, it is of great interest if they also have chemoeffector potential. Besides pyoverdine, which was proved to be a repellent for *E. coli*, there can be other unidentified chemoeffectors that may initiate the observed negative chemotactic response. On the other hand, some of these secreted chemical compounds can act as attractants, just as the AHL signals or pyocyanin. Thus, observations in our co-culturing experiments may be a result of a net chemotactic response to several simultaneous chemoeffector gradients. Exploring the chemoeffector

potential of further bacterial communication signals that may also affect the spatial pattern formation of cells could be the object of future studies.

In light of the results obtained using pyoverdine, pyocyanin, and AHL gradients, a population level interaction between adjacent bacterial colonies may be quite complex. The dynamic pattern formations in our microfluidic device are a result of the interplay between several chemical clues, even opposing, attractant or repellent effects.

CONCLUSION

We have introduced a flow-free microfluidic device to create linear chemical concentration gradients, and probe the chemotactic behavior of *E. coli* bacteria in various conditions. We have quantitatively characterized the gradients formed in the microdevice and showed both with model calculations and experiments that these gradients can be precisely engineered. We demonstrated that gradients form in our device under 3 min, which is considerably faster than the times reported for other flow-free devices.^{42–44,46,47} This makes the device suitable to study the dynamics of bacterial chemotaxis in chemoeffector gradients. We also demonstrated that after a fast formation, the gradients in the device stay stable for more than 24 h, making long term chemotaxis experiments possible.

In *E. coli* chemotaxis experiments, we have shown that well-known chemoeffectors induce the expected spatial rearrangements of the cells in the device. Furthermore, we have tested the chemoeffector potential of two amino acids and several chemical compounds related to *P. aeruginosa* quorum sensing. We have shown that the amino acid L-lysine acts as a weak attractant, while L-arginine does not induce a chemotactic response by *E. coli*.

C4-HSL and oxo-C12-HSL, the two main signal molecules used in *P. aeruginosa* quorum sensing are proved to be chemoattractants for *E. coli*. C4-HSL is a stronger attractant than oxo-C12-HSL; however, for both compounds the chemotactic response seems to be transient and diminish or considerably weaken after a few hours.

Pyocyanin and pyoverdine are redox-active secondary metabolites that are linked to the quorum sensing mechanisms in *P. aeruginosa*. We have shown that pyocyanin is a weak attractant, while pyoverdine are somewhat stronger repellent for *E. coli*. The chemotactic response to pyocyanin is transient, but it is more prolonged compared to pyoverdine. Further studies are needed to reveal the exact mechanism behind the chemotactic response to L-lysine, AHLs, pyocyanin, and pyoverdine. For example, it is not known if any of the four typical chemosensory proteins of *E. coli* has an affinity to these compounds. Although the SdiA receptor in *E. coli* interacts with AHLs, it has not been shown that this affects chemotaxis. The response to lysine is similar to other known attractant amino acids (e.g., aspartate) only slower and weaker. On the other hand, the chemotactic response to AHLs and secondary metabolites is markedly different as the effect of these compounds seems to be temporary. It is an interesting question what leads to such a transitional response. It is known that adaptation mechanisms alter the sensitivity of chemoreceptors. This process has the function to span the useful concentration range in which chemotaxis works. However, it has not been demonstrated before that an adaptation like process would lead to temporal chemotactic response.

The abovementioned results demonstrate that signal molecules and metabolic products of one bacterial strain induce a chemotactic response of another strain. In multispecies, bacterial communities such interspecies interactions may have an important role in the organization and function of the community. To demonstrate this on a basic level, we performed co-culturing experiments and showed that a complex biochemical interaction shapes the spatial distribution of neighboring populations. A *P. aeruginosa* culture growing in a nutrient rich environment attracts the neighboring *E. coli* population. Unidentified factors, however, induce the surface adhesion of *E. coli* bacteria in the vicinity of the *Pseudomonas* culture, indicating that these factors could be secreted by the *P. aeruginosa* cells. In a few hours, a planktonic subpopulation is repelled by the *Pseudomonas* colony.

Although the primary habitat for *E. coli* is the gastrointestinal tract of warm blooded animals, the secondary habitats, like soil, water, and sediments, are shared with *P. aeruginosa*.⁶⁴

Therefore, these bacteria may live side by side and interact in these natural environments, but the specific benefits of *E. coli* chemotaxis to AHLs and secondary metabolites are yet unclear. In general, we can say, that biochemical interaction between bacterial populations is a complex phenomena in which numerous secreted compounds play a role. Our results suggest that signal molecules and secondary metabolites connected to quorum sensing are also among the potentially important chemicals that may act throughout the induction of a chemotactic response. Although the exact mechanisms are not clear yet, these phenomena may shape multispecies bacterial communities.

ACKNOWLEDGMENTS

We are grateful to Karen Fahrner and Howard C. Berg for providing the *E. coli* strains. We thank Vittorio Venturi, Iris Bertani, and Sándor Pongor for providing us the *P. aeruginosa* strain. This work was supported by the “Lendület” Program of the Hungarian Academy of Sciences and the OTKA NN102624 and PD OTKA 112509 Hungarian research grants.

- ¹J. Adler, *Science* **153**, 708 (1966).
- ²H. C. Berg, *E. coli in Motion* (Springer-Verlag, 2003).
- ³G. Dunny and S. Winans, *Cell-Cell Signaling in Bacteria* (ASM Press, 1999).
- ⁴C. M. Waters and B. L. Bassler, *Annu. Rev. Cell. Dev. Biol.* **21**, 319 (2005).
- ⁵C. Fuqua, M. R. Parsek, and E. P. Greenberg, *Annu. Rev. Genet.* **35**, 439 (2001).
- ⁶B. Bassler and R. Losick, *Cell* **125**, 237 (2006).
- ⁷D. L. Englert, M. D. Manson, and A. Jayaraman, *Appl. Environ. Microbiol.* **75**, 4557 (2009).
- ⁸S. Park, P. Wolanin, E. Yuzbashyan, H. Lin, N. Darnton, J. Stock, P. Silberzan, and R. Austin, *Proc. Natl. Acad. Sci. U. S. A.* **100**, 13910 (2003).
- ⁹M. Hegde, D. L. Englert, S. Schrock, W. B. Cohn, C. Vogt, T. K. Wood, M. D. Manson, and A. Jayaraman, *J. Bacteriol.* **193**, 768 (2011).
- ¹⁰B. A. Rader, C. Wreden, K. G. Hicks, E. G. Sweeney, K. M. Ottemann, and K. Guillemin, *Microbiology* **157**, 2445 (2011).
- ¹¹S. M. Butler and A. Camilli, *Proc. Natl. Acad. Sci. U. S. A.* **101**, 5018 (2004).
- ¹²K. Terry, S. M. Williams, L. Connolly, and K. M. Ottemann, *Infect. Immun.* **73**, 803 (2005).
- ¹³T. Bansal, D. Englert, J. Lee, M. Hegde, T. K. Wood, and A. Jayaraman, *Infect. Immun.* **75**, 4597 (2007).
- ¹⁴T. R. De Kievit and B. H. Iglewski, *Infect. Immun.* **68**, 4839 (2000).
- ¹⁵K. Winzer and P. Williams, *Int. J. Med. Microbiol.* **291**, 131 (2001).
- ¹⁶R. S. Smith and B. H. Iglewski, *Curr. Opin. Microbiol.* **6**, 56 (2003).
- ¹⁷M. J. Gambello and B. H. Iglewski, *J. Bacteriol.* **173**, 3000 (1991).
- ¹⁸L. Passador, J. Cook, M. Gambello, L. Rust, and B. Iglewski, *Science* **260**, 1127 (1993).
- ¹⁹J. Pearson, L. Passador, B. Iglewski, and E. Greenberg, *Proc. Natl. Acad. Sci. U. S. A.* **92**, 1490 (1995).
- ²⁰M. K. Winson, M. Camara, A. Latifi, M. Foglino, S. R. Chhabra, M. Daykin, M. Bally, V. Chapon, G. P. Salmond, B. W. Bycroft, A. Lazdunski, G. S. Stewart, and P. Williams, *Proc. Natl. Acad. Sci. U. S. A.* **92**, 9427 (1995).
- ²¹N. Whitehead, A. Barnard, H. Slater, N. Simpson, and G. Salmond, *FEMS Microbiol. Rev.* **25**, 365 (2001).
- ²²B. Ahmer, *Mol. Microbiol.* **52**, 933 (2004).
- ²³R. Houdt, A. Aertsen, P. Moons, K. Vanoirbeek, and C. W. Michiels, *FEMS Microbiol. Lett.* **256**, 83 (2006).
- ²⁴J. Lee, T. Maeda, S. H. Hong, and T. K. Wood, *Appl. Environ. Microbiol.* **75**, 1703 (2009).
- ²⁵S. S. Baron and J. J. Rowe, *Antimicrob. Agents Chemother.* **20**, 814 (1981).
- ²⁶H. Cao, G. Krishnan, B. Goumnerov, J. Tsongalis, R. Tompkins, and L. G. Rahme, *Proc. Natl. Acad. Sci. U. S. A.* **98**, 14613 (2001).
- ²⁷L. E. P. Dietrich, A. Price-Whelan, A. Petersen, M. Whiteley, and D. K. Newman, *Mol. Microbiol.* **61**, 1308 (2006).
- ²⁸I. J. Schalk, C. Hennard, C. Dugave, K. Poole, M. A. Abdallah, and F. Pattus, *Mol. Microbiol.* **39**, 351 (2001).
- ²⁹V. Braun, *Biol. Chem.* **378**, 779 (1997).
- ³⁰C. Ratledge and L. G. Dover, *Annu. Rev. Microbiol.* **54**, 881 (2000).
- ³¹T. Ahmed, T. S. Shimizu, and R. Stocker, *Integr. Biol.* **2**, 604 (2010).
- ³²H. Mao, P. S. Cremer, and M. D. Manson, *Proc. Natl. Acad. Sci. U. S. A.* **100**, 5449 (2003).
- ³³L. M. Lanning, R. M. Ford, and T. Long, *Biotechnol. Bioeng.* **100**, 653 (2008).
- ³⁴R. Stocker, J. R. Seymour, A. Samadani, D. E. Hunt, and M. F. Polz, *Proc. Natl. Acad. Sci. U. S. A.* **105**, 4209 (2008).
- ³⁵H. Jeon, Y. Lee, S. Jin, S. Koo, C.-S. Lee, and J. Y. Yoo, *Biomed. Microdevices* **11**, 1135 (2009).
- ³⁶T. Ahmed and R. Stocker, *Biophys. J.* **95**, 4481 (2008).
- ³⁷T. Kim, M. Pinelis, and M. M. Maharbiz, *Biomed. Microdevices* **11**, 65 (2009).
- ³⁸J. J. VanDersarl, A. M. Xu, and N. A. Melosh, *Lab Chip* **11**, 3057 (2011).
- ³⁹J. Diao, L. Young, S. Kim, E. A. Fogarty, S. M. Heilman, P. Zhou, M. L. Shuler, M. Wu, and M. P. DeLisa, *Lab Chip* **6**, 381 (2006).
- ⁴⁰H. Wu, B. Huang, and R. N. Zare, *J. Am. Chem. Soc.* **128**, 4194 (2006).
- ⁴¹S.-Y. Cheng, S. Heilman, M. Wasserman, S. Archer, M. L. Shuler, and M. Wu, *Lab Chip* **7**, 763 (2007).
- ⁴²T. Ahmed, T. S. Shimizu, and R. Stocker, *Nano Lett.* **10**, 3379 (2010).
- ⁴³M. Kim and T. Kim, *Anal. Chem.* **82**, 9401 (2010).
- ⁴⁴G. Si, W. Yang, S. Bi, C. Luo, and Q. Ouyang, *Lab Chip* **12**, 1389 (2012).
- ⁴⁵Y. Zhou and Q. Lin, *Sens. Actuators B* **190**, 334 (2014).

- ⁴⁶U. Haessler, Y. Kalinin, M. A. Swartz, and M. Wu, *Biomed. Microdevices* **11**, 827 (2009).
- ⁴⁷J. W. Hong, S. Song, and J. H. Shin, *Lab Chip* **13**, 3033 (2013).
- ⁴⁸D. Qin, Y. Xia, and G. M. Whitesides, *Nat. Protoc.* **5**, 491 (2010).
- ⁴⁹B.-H. Chueh, D. Huh, C. R. Kyrtos, T. Houssin, N. Futai, and S. Takayama, *Anal. Chem.* **79**, 3504 (2007).
- ⁵⁰A. J. Wolfe and H. C. Berg, *Proc. Natl. Acad. Sci. U. S. A.* **86**, 6973 (1989).
- ⁵¹M. P. Mayer, *Gene* **163**, 41 (1995).
- ⁵²R. Kumar, N. Ayyadurai, P. Pandiaraja, A. Reddy, Y. Venkateswarlu, O. Prakash, and N. Sakthivel, *J. Appl. Microbiol.* **98**, 145 (2005).
- ⁵³C. A. Schneider, W. S. Rasband, and K. W. Eliceiri, *Nat. Methods* **9**, 671 (2012).
- ⁵⁴K. Nagy, O. Sipos, É. Gombai, Á. Kerényi, S. Valkai, P. Ormos, and P. Galajda, *Chem. Biochem. Eng. Q.* **28**, 225 (2014).
- ⁵⁵R. Mesibov and J. Adler, *J. Bacteriol.* **112**, 315 (1972).
- ⁵⁶W. W. Tso and J. Adler, *J. Bacteriol.* **118**, 560 (1974).
- ⁵⁷T. S. Charlton, R. de Nys, A. Netting, N. Kumar, M. Hentzer, M. Givskov, and S. Kjelleberg, *Environ. Microbiol.* **2**, 530 (2000).
- ⁵⁸P. Visca, L. Leoni, M. J. Wilson, and I. L. Lamont, *Mol. Microbiol.* **45**, 1177 (2002).
- ⁵⁹P. A. Beare, R. J. For, L. W. Martin, and I. L. Lamont, *Mol. Microbiol.* **47**, 195 (2003).
- ⁶⁰A. Stintzi, K. Evans, J. M. Meyer, and K. Poole, *FEMS Microbiol. Lett.* **166**, 341 (1998).
- ⁶¹R. Xiao and W. S. Kisaalita, *Appl. Environ. Microbiol.* **61**, 3769 (1995).
- ⁶²M. T. Holden *et al.*, *Mol. Microbiol.* **33**, 1254 (1999).
- ⁶³Y. Tashiro, S. Ichikawa, T. Nakajima-Kambe, H. Uchiyama, and N. Nomura, *Microbes Environ.* **25**, 120 (2010).
- ⁶⁴M. A. Savageau, *Am. Nat.* **122**, 732 (1983).